Available online at www.sciencedirect.com
SCIENCE DIRECT®
Journal of Solid State Chemistry 179 (2006) 404–412
JOURNAL OF SOLID STATE CHEMISTRY
www.elsevier.com/locate/jssc

Old friends in a new light: "SnSb" revisited

Lasse Norén[a,*], Ray L. Withers[a], Siegbert Schmid[b], Frank J. Brink[a,1], Valeska Ting[a]

[a]*Research School of Chemistry, Australian National University, Canberra, ACT 0200, Australia*
[b]*School of Chemistry, Building F11, University of Sydney, NSW 2006, Australia*

Received 30 August 2005; received in revised form 17 October 2005; accepted 23 October 2005
Available online 1 December 2005

Abstract

The binary pnictide 'SnSb' has been re-investigated using a combination of X-ray, synchrotron and electron diffraction as well as electron microprobe analysis. Its structure was found to be incommensurately modulated with an underlying rhombohedral parent structure of space group symmetry $R\bar{3}m$ (No. 166), unit cell parameters $a_h = b_h = 4.3251(4)$ Å, $c_h = 5.3376(6)$ Å in the hexagonal setting. The incommensurate primary modulation wave vector $\mathbf{q}_h = 1.3109(9)\mathbf{c}_h^*$ and the superspace group symmetry is $R\bar{3}m$ (0, 0, ~1.311) (No. 166.1). The refinement of the incommensurate structure indicates that the satellite reflections arise from displacive shifts of presumably essentially pure Sn and Sb layers along the hexagonal *c*-axis, with increasing distance between the Sn-layers and decreasing distance between the Sb layers.

Keywords: SnSb; Incommensurately modulated structure; Synchrotron data; TEM

1. Introduction

Antimony (Sb) and tin (Sn) are elements known to mankind from antiquity. Plinius the Elder referred to the sulphide of Sb as *stimi* [1], *stibium* in Latin. In subsequent Arabic texts, the same material was referred to as *al-ithmīd*, an Arabicization of the Latin name. When these texts were later translated back to Latin, the latinized form for *al-ithmīd* ended up as *antimonium* [2]. A method for making metallic Sb was first described by Al-Razi (a.k.a. Rhazes) and later by Georg Bauer (a.k.a. Georgius Agricola) [3]. Johann Thölde (a.k.a. Basilius Valentinus) devoted a whole book to the element [4].

Sn, on the other hand, is one of the oldest known metals (being easily reduced from the oxide in glowing coals) and dating back to ~3500 BCE (Before the Common Era) when it was used in combination with copper to form bronze. It was later used in combination with lead to form solder as detailed by Plinius the Elder [5]. It is therefore of interest to note that Sn–Sb-based alloys have recently emerged as serious candidate materials in the search for a lead-free solder to use in today's electronics industry [6–8]. Sn–Sb alloys furthermore have metallurgical uses, for instance as components in bearings [9], and have recently also been proposed as cathode materials for use in lithium ion batteries [10,11].

The exact composition and structure of 'SnSb' (the so-called β-phase) has been a source of controversy from the earliest days of X-ray crystallography [7,12–20]. Its structure has been variously described as primitive cubic (a~3.05 Å) [12], of *NaCl* structure type (a~6.13 Å) [13–15] and as rhombohedral (a_{rho}~6.13 Å, α_{rho}~89.6°) [16–18]. The phase also occurs in nature as the mineral "*stistaite*" and was first discovered as an inclusion in native Sn by Nikolaeva et al. [19] in 1970. Its structure was described differently again therein, this time as body centred cubic with $a = 4.15$ Å. A later revision of the mineral by Rose [20], based on samples from Colombia, reported that the structure of *stistaite* (containing 0.23% Cu) is in fact rhombohedral ($a_{rho} = 6.131$ Å, $\alpha_{rho} = 89.70°$ or, in the hexagonal setting, $a_{hex} = 8.648$ Å, $c_{hex} = 10.675$ Å), in line

*Corresponding author. Fax: +61 2 6125 3218.
E-mail address: Ray.Withers@anu.edu.au (R.L. Withers).
[1]Also at Electron Microscopy. Unit, Australian National University, Canberra, ACT 0200 Australia.

0022-4596/$ - see front matter © 2005 Elsevier Inc. All rights reserved.
doi:10.1016/j.jssc.2005.10.031

with the conclusions drawn from the synthesized samples [16–18].

The initial phase diagram of the Sn–Sb system by Guertler (reported in [15]; see Fig. 1a) reported two intermediate solid solution phases, the first ranging from 40% to 44% Sb and the second from 50% to 56% Sb. Subsequent work around the same period reported a single intermediary "SnSb", or β-phase encompassing an extended $Sn_{1-x}Sb_{1+x}$ homogeneity range including the nominally ideal SnSb composition [12–16]. Significant variability in the extent of this solid solution range (as well as of the binary phase diagram—see Fig. 1) have been reported over the years [7,13–18]. Bowen and Morris Jones [15], for example, reported a composition range from $Sn_{0.60}Sb_{0.40}$ to $Sn_{0.46}Sb_{0.54}$ (see Fig. 1b) while Hägg and Hybinette [16] reported a composition range from $Sn_{0.55}Sb_{0.45}$ to $Sn_{0.45}Sb_{0.55}$ (see Fig. 1c).

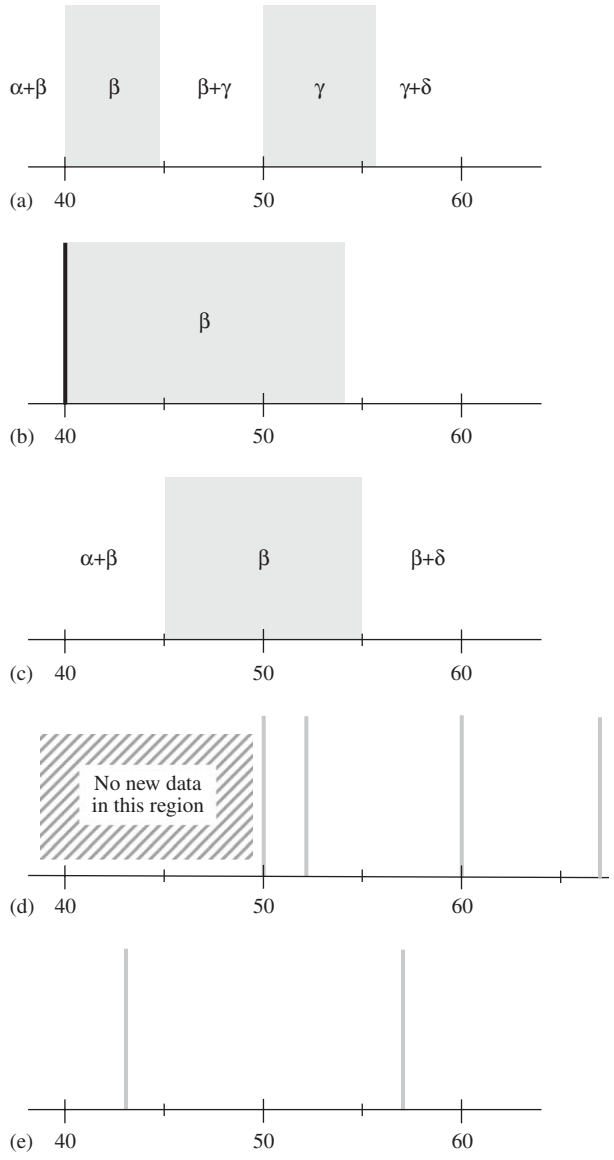

Fig. 1. Shows some of the various Sn–Sb binary phase diagrams reported in the literature around the 'SnSb', β-phase area of interest. (a) the initial phase diagram of the Sn–Sb system by Guertler (reported in [15]), (b) from Bowen and Morris Jones [15], (c) from Hägg and Hybinette [16], (d) from Vassiliev et al. [18] and (e) from Obendorff et al [7]. See the text for details.

In a more recent study, Vassiliev et al. [18] used electromotive force (e.m.f) measurements combined with X-ray powder diffraction to study the system and concluded that the 'SnSb' (or β-phase) solid solution did not exist as such and should instead be separated into four distinct, almost line-phase like compounds of stoichiometry "SnSb", "$Sn_{12}Sb_{13}$", "Sn_2Sb_3" and "$SnSb_2$" (their study did not include the Sn-rich area of the 'solid solution', see Fig. 1d). They further suggested that any variation in stoichiometry would be governed by the stacking sequence of Sn- and Sb-layers along the crystallographic c-axis (in the hexagonal setting) as well as by substitution of Sn-atoms onto Sb-atom positions in the Sb-layers [18].

In a more recent study still [7], on the ternary system Ag–Sn–Sb using electron probe microanalysis (EPMA), the authors conclude that the composition SnSb "…is unlikely to exist at 220 °C…", the only compositions they found being Sn_4Sb_3 ($Sn_{0.57}Sb_{0.43}$) and Sn_3Sb_4 ($Sn_{0.43}Sb_{0.57}$), see Fig. 1e. Note that naturally occurring *stistaite* is reported to have the general composition $Sn_{0.561}Sb_{0.437}Cu_{0.002}$ [20].

Given these rather variable structural and compositional reports, it was felt that it was time for a careful re-investigation of this system via a combined diffraction and microprobe analysis study.

2. Experimental

2.1. Synthesis

A phase with nominal composition SnSb was made by reacting stoichiometric amounts of Sn (4N) and Sb (5N) in evacuated borosilicate glass tubes. The reactants were heated until a uniform melt was obtained and then slowly quenched in air. The product was then heated at 270 °C for 3 months. The weight-loss at the end of this heat treatment was well below 0.1%. The average composition of the sample was therefore assumed to be SnSb (Sample A). A small part of this sample was placed in an evacuated silica tube and heated until molten and then rapidly quenched in water (Sample B).

2.2. Electron probe microanalysis (EPMA)

The homogeneity and composition of these samples were quantitatively analysed via EPMA using a JEOL 6400 scanning electron microscope (SEM) equipped with an Oxford Instruments light element EDS detector and Link ISIS SEMquant software. The samples were embedded in resin and polished to a $<1\,\mu m$ finish with corundum. Multiple spot analyses as well as X-ray mapping were carried out at 15 kV and 1 nA using the pure elements as calibration standards. The reported results are based on the average of a series of spot analyses as well as quantitative X-ray mapping.

2.3. X-ray diffraction

Laboratory X-ray diffraction (XRD) data were obtained using a Guinier–Hägg focusing camera with Cu$K\alpha_1$ radiation. Silicon (NBS 640) was used as an internal standard for accurate determination of unit cell parameters, refined using the "Unitcell" software package [21]. Synchrotron X-ray powder diffraction patterns were also collected at the Australian National Beamline Facility (ANBF) at the Photon Factory, Tsukuba, Japan, with a wavelength of 0.75026 Å. Silicon was used as an internal standard for the precise wavelength determination. The intensity of the strongest peak in the diffraction pattern of Sample A was truncated when the image plate was read and thus that peak is excluded from the refinement.

2.4. Electron diffraction

Crushed specimens of the 'SnSb' samples were deposited onto holey-carbon coated copper grids and examined in a Philips EM 430 Transmission Electron Microscope (TEM).

3. Results

3.1. Electron probe microanalysis (EPMA)

The rapidly quenched Sample B specimen was found to be reasonably homogeneous in composition and showed no evidence for micro-phases of distinct composition condensing out. The average composition was $Sn_{0.51(3)}Sb_{0.49(3)}$ with a relatively narrow, although still noticeable, composition spread ranging from $\sim Sn_{48}Sb_{52}$ to $\sim Sn_{53}Sb_{47}$. The long-term annealed Sample A specimen showed a significantly broader spread in composition suggesting that several distinct micro-phases might be attempting to condense out. Fig. 2, for example, shows an X-ray map (obtained from ~47,000 separate 2 s analyses) of a large area of Sample A. A distinct variability in composition around the ideal 50:50 composition is apparent. The extremes in this composition range are marked on Fig. 2. Some two hundred, 100 s spot analyses over the same area confirmed the composition spread apparent in the X-ray map. Clearly 'equilibrium' is rather difficult to achieve in this system.

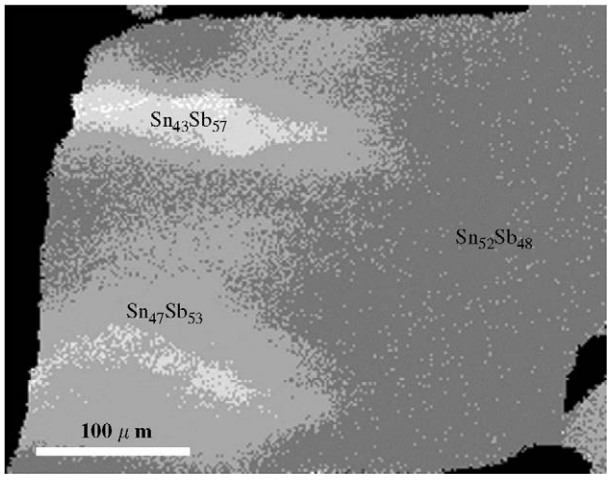

Fig. 2. X-ray map of a large area of Sample A (obtained from ~47,000 separate 2 s analyses). The extremes in this composition range are marked.

3.2. XRD

Laboratory as well as synchrotron XRD data (see Fig. 3) unambiguously confirmed rhombohedral, although very close to cubic, metric symmetry for the underlying average structures of both the 'SnSb' samples, i.e. for both the 3 month annealed Sample A specimen ($a_h = b_h = 4.3253(8)$, $c_h = 5.3384(12)$ Å, in the hexagonal setting—see Fig. 3b and d; $a_R = 3.0664$ Å, $\alpha_R = 89.705°$ in the rhombohedral setting) as well as for the rapidly quenched Sample B ($a_h = b_h = 4.3226(8)$, $c_h = 5.3398(15)$ Å, in the hexagonal setting—see Fig. 3a and c; $a_R = 3.0654$ Å, $\alpha_R = 89.671°$ in the rhombohedral setting). The $(3+1)$ integer $hklm_h$ ($\equiv ha_h^* + kb_h^* + lc_h^* + mq_h^*$) indexation with the subscript h in Figs. 3c and d is with respect to the hexagonal setting. The relationship between the unit cells of the two rhombohedral settings is given by $\mathbf{a}_R = \frac{1}{3}(-\mathbf{a}_h - 2\mathbf{b}_h + \mathbf{c}_h)$, $\mathbf{b}_R = \frac{1}{3}(2\mathbf{a}_h + \mathbf{b}_h + \mathbf{c}_h)$ and $\mathbf{c}_R = \frac{1}{3}(-\mathbf{a}_h + \mathbf{b}_h + \mathbf{c}_h)$, respectively (in reciprocal space $\mathbf{a}_R^* = [0\bar{1}1]_h^*$, $\mathbf{b}_R^* = [101]_h^*$ and $\mathbf{c}_R^* = [\bar{1}11]_h^*$). Apart from the very slight deviation from cubic metric symmetry, this necessarily primitive, essentially simple cubic lattice (containing only one mixed metal atom, 1*a* site per unit cell in the (primitive) rhombohedral setting) is virtually the same as that reported by Osawa [12]. Note that the virtually identical X-ray scattering factors of Sn and Sb (Sn and Sb are neighbouring elements in the Periodic Table) mean that Sn/Sb ordering is very difficult to detect by means of X-ray diffraction data.

Some additional reflections (see the top row of reflection markers in Figs. 3a and c) were observed in the synchrotron X-ray data from the rapidly quenched Sample B collected soon after synthesis which did not fit to the above 'SnSb', β-phase cell. They were subsequently identified as belonging to the "white" (metallic) form of elemental Sn. Upon re-investigation after several months, these same Sn reflections were no longer present in Guinier–Hägg X-ray data (see Table 1). Nor was the presence of Sn, or overall Sn deficiency in the 'SnSb' phase, detected in EPMA data from Sample B (see above). Sn reflections were never detected in the 3 months annealed Sample A, either in the Guinier–Hägg films or in the synchrotron data. Very weak additional incommensurate satellite reflections (see the Electron Diffraction section below) were, however, observed (see Fig. 3b and d). The same incommensurate satellite reflections are in fact still present, although significantly broadened and barely detectable, in the synchrotron data of Sample B (arrowed in Fig. 3c). The presence of these incommensurate satellite reflections in Sample B was also confirmed by electron diffraction, see below.

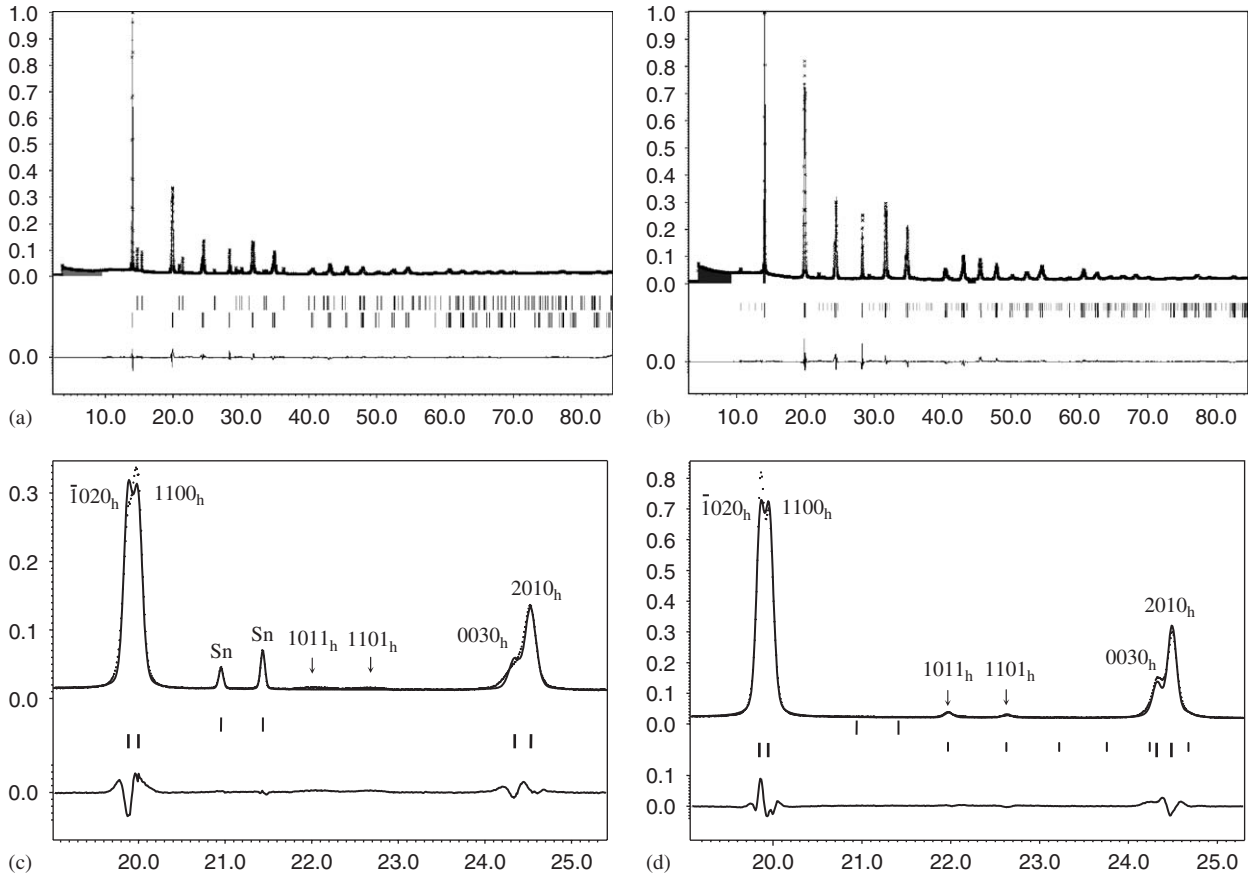

Fig. 3. The refined synchrotron X-ray powder patterns of (a) quenched 'SnSb' (Sample B) and (b) the incommensurately modulated Sample A. A blow-up of the low angle portion of the first pattern (c) clearly shows the presence of a small amount of a second phase (the upper tick marks), corresponding to β-Sn. A blow-up of the same portion for Sample A (d) shows that the second β-Sn phase is missing while additional sharp incommensurate satellite reflections, however, are now clearly visible.

Table 1
Unit cell parameters (in Ångström, Å) and relevant refinement statistics for the various refinements of the Sample A and B, 'SnSb' compounds

	a	c	Phase fraction	R_p	R_{wp}	GoF
Sample A	4.3249(16)	5.337(2)	1	5.92	8.21	1.47
	4.3254(18)	5.335(3)	1			
	4.3237(8)	5.3359(9)	1	4.79	6.55	1.18
Sample B	4.3239(2)	5.3418(5)	0.914(5)	5.05	6.99	1.00
	4.3289(5)	5.3467(6)				
Tin	5.8377(6)	3.1809(4)	0.086(5)	5.05	6.99	1.00
	5.8317	3.1815	1 [28]			

The first line in each case is obtained from the average structure Rietveld refinements. The second line for Samples A and B corresponds to Guinier–Hägg data using Cu$K\alpha_1$ radiation. The third line for Sample A corresponds to the incommensurate structure refinement. For the Sn-phase, the second line is data from the literature [28].

The sharp incommensurate satellite reflections in the case of Sample A could all be indexed using a very well-defined primary modulation wave-vector of $\mathbf{q}_h = 1.3109(9)^*_c$ (despite the EPMA evidence for somewhat variable local composition), when indexed with respect to the hexagonal setting of the $R\bar{3}m$ average structure unit cell, or $\mathbf{q}_R = 0.4370(3)[111]^*_R$, when indexed with respect to the rhombohedral setting of the $R\bar{3}m$ average structure cell. This is in excellent agreement with the data obtained in the TEM investigation (see below).

The synchrotron X-ray powder diffraction data were refined via profile analysis using the program package Jana2000 [22,23]. The somewhat variable local composition apparent in the EPMA data (particularly for the long-

term annealed Sample A specimen) had to be ignored for this purpose. Incommensurate satellite reflections are observed for both samples, albeit very broad and weak ones for Sample B. Given the weakness of all satellite reflections, $R\bar{3}m$ average structure refinements were carried out initially. The background was fitted using a Legendre polynomial with 12 refinable parameters. The half-width parameters were modelled using 3 parameters with one parameter for the Lorentzian contribution, one global shift parameter as well as one further asymmetry parameter.

The other parameters refined were the unit cell dimensions and the isotropic atomic displacement parameter (ADP) of the Sn/Sb atom. (Note that there exists only one atom site in the asymmetric unit of the $R\bar{3}m$ average structure unit cell—a mixed metal atom, 3*a* site in the hexagonal setting, at 0 0 0). For Sample B, a relative phase scale (SnSb/Sn) with its accompanying occupancy was refined as well. Excluded regions were used for the beginning of the patterns (where the effect of the glass capillary were most noticeable but no sample reflections existed) as well as in the region where the image plates overlapped. One further excluded region was necessary for Sample A since the strong $(101)_h$ reflection had saturated the image plate. Reasonable quality fits were obtained for both Sample A ($R_p = 0.0592$, $R_{wp} = 0.0821$, g.o.f. = 1.47, $R_{Obs} = 0.0535$, $R_{wObs} = 0.0455$ for 79 calculated main reflections) as well as for Sample B ($R_p = 0.0502$, $R_{wp} = 0.0699$, g.o.f. = 1.00, $R_{Obs} = 0.0568$, $R_{wObs} = 0.0431$).

Only for Sample A did it prove possible to carry out refinement of the incommensurate structure ($R_p = 0.0479$, $R_{wp} = 0.0655$, g.o.f. = 1.18, $R_{Obs} = 0.0562$, $R_{wObs} = 0.0450$), likely due to the broadening of the satellite reflections caused by rapid quenching in the case of Sample B, see below. Both main reflections and first order satellite reflections were included in the refinement ($R_m = 0.0404$, $R_{mw} = 0.0384$ (79 reflections), $R_{1st} = 0.0880$, $R_{1stw} = 0.0642$). Note that the overall $R\bar{3}m$ (0,0,~1.311) superspace group symmetry (see below) allows both compositional (Sn/Sb) modulation as well as *c*-axis displacement of the metal atom layers. The amplitude of this sin*z* displacement of the metal atoms refined to a magnitude of −0.0223(6) *c* (≡ a maximum shift magnitude of 0.12 Å). The results and refinement statistics are given in Table 1. The final profile fit for the average structure of Sample B is shown in Fig. 3a while that for the incommensurately modulated structure of Sample A is shown in Fig. 3b. A modulation wave approach (see below) suggests the origin for the observed incommensurate satellite reflections is essentially Sn/Sb ordering in layers perpendicular to $\mathbf{c}_h$ and associated displacive relaxation.

3.3. Electron diffraction

Fig. 4 shows (a) $[11\bar{2}]_R \equiv [1\bar{1}0]_h$ and (b) $[\bar{1}10]_R \equiv [110]_h$ zone axis electron diffraction patterns (EDPs) typical of the "SnSb" phase for both Sample A as well as Sample B. Three integer indexation with the subscript R in Fig. 4 is with respect to the rhombohedral setting unit cell given above while the (3 + 1) integer (*hklm*) indexation with the subscript h is with respect to the hexagonal setting unit cell also given above. Accompanying the strong Bragg reflections of the underlying rhombohedral ($R\bar{3}m$) average structure unit cell (corresponding to those reflections with $m = 0$ in Fig. 4, and labelled **G** hereinafter), note the clear presence in each case of additional incommensurate $\mathbf{G} \pm m\mathbf{q}$ satellite reflections ($m = 1, 2, \ldots$ and primary modulation wave-vector $\mathbf{q} \sim 0.435(3)\ [111]^*_R \equiv 0.435(3)[003]^*_h$).

In the case of Sample A, in agreement with the sharp satellite reflections apparent in the synchrotron XRD data,

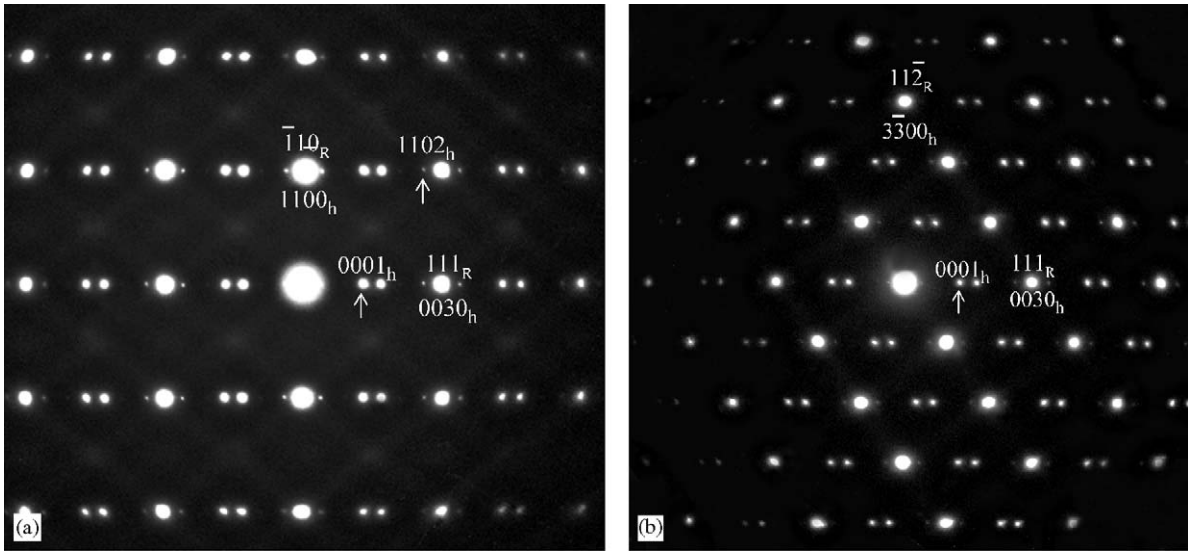

Fig. 4. (a) $[11\bar{2}]_R \equiv [1\bar{1}0]_h$ and (b) $[\bar{1}10]_R \equiv [110]_h$ zone axis EDPs typical of the "SnSb" phase for both Sample A as well as Sample B. Three integer indexation with the subscript R is with respect to the rhombohedral setting unit cell while the (3 + 1) integer (*hklm*) indexation with the subscript h is with respect to the hexagonal setting unit cell.

no variability at all in the magnitude of the incommensurate primary modulation wave-vector $q = 0.435(3)$ was ever detected in the many EDPs equivalent to those shown in Fig. 4 taken from different grains. This is a remarkable result given the local compositional variability around the ideal 50:50 apparent in the EPMA data (see Fig. 2). It suggests that **q** cannot be acting as a strict 'chemical ruler', i.e. is not a strict function of the local composition, and suggests that there may in fact be some other, perhaps Fermi surface driven, explanation for the reproducibility of the magnitude of the incommensurate primary modulation wave-vector.

In the case of Sample B, again in agreement with the broadened satellite reflections apparent in the synchrotron XRD data (cf. Fig. 3c with 3d), some (although strictly limited) variability in the magnitude of the incommensurate primary modulation wave-vector q was detected, e.g. in one grain q was measured as 0.449(2) instead of 0.435(3). This $\pm\sim$2–3% limited variability in q is consistent with the extent of the observed broadening of the incommensurate satellite reflections in the synchrotron X-ray data of Sample B.

It is also consistent with an increased prevalence of orientational twinning in the case of Sample B (see e.g. Fig. 5a), hardly surprising given the rhombohedral but very close to cubic metric symmetry of the underlying parent structure. In EDPs such as Fig. 5a, this orientational twinning gives rise to an apparent cluster of 4 incommensurate satellite reflections surrounding each parent structure reciprocal lattice cell. The two sets of twin variant reflections comprising this overall composite EDP are labelled with superscripts 1 and 2 respectively in Fig. 5a. The systematic change in shape of the cluster of 4 incommensurate satellite reflections along the '$\langle 001\rangle^*_R$' direction but not along the $\langle 110\rangle^*_R$ direction requires that $[110^1_R]^*$ coincides with $[110^2_R]^*$ while the $[001^1_R]^*$ and $[00\bar{1}^1_R]^*$ reflections are then necessarily narrowly split along the $[110^{1,2}_R]^*$ direction of reciprocal space.

The fact that the incommensurate satellite reflections run along only one of the four, initially symmetry equivalent $[111]^*_p$ (p for simple cubic, $Pm\bar{3}m$ ideal parent structure) reciprocal lattice directions in single domain EDPs makes that particular $[111]^*_p$ reciprocal space direction unique and accounts for the observed rhombohedral symmetry of the underlying average structure. The traditional assumption of a *NaCl* structure-type arrangement of Sn and Sb atoms [13–16] provides no explanation for the observed rhombohedral metric symmetry. By contrast, the later assumption of Vassiliev et al. [18] of $(001)_h$ layers of either essentially Sn or essentially Sb type does provide a potential explanation for the observed rhombohedral metric symmetry. In addition, allowing the stacking sequence of these proposed essentially Sn and essentially Sb layers to vary along the $\mathbf{c}_h$ direction (which was done in order to explain the observed composition variations of 'SnSb') also provides a potential explanation for the observed incommensurate satellite reflections.

Given $R\bar{3}m$ average structure space group symmetry, there is only one possible (3 + 1)−d incommensurate superspace group symmetry [24] compatible with the above experimental observations (i.e. with the absence of any non-Bravais lattice-type systematic extinction conditions)—namely $R\bar{3}m$ (0,0,∼1.311) (No. 166.1 in Table 9.8.3.35 of the superspace group tables of Ref. [24]). The

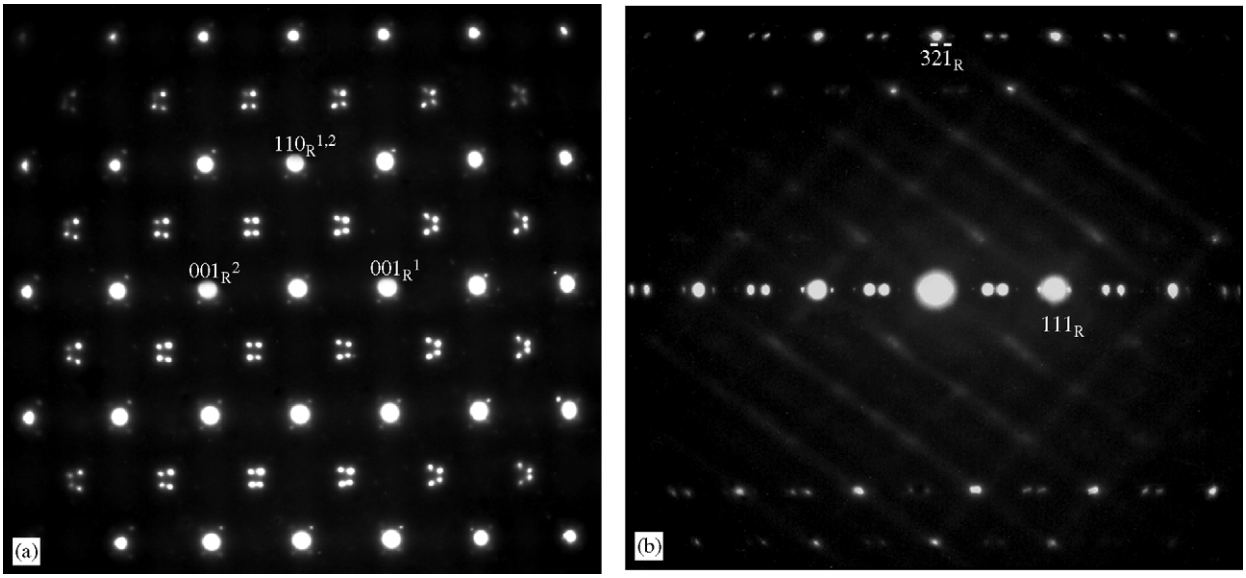

Fig. 5. (a) A$\langle\bar{1}10\rangle_R \equiv \langle 110\rangle_h$ zone axis EDP of Sample B showing orientational twinning. The orientational twinning gives rise to an apparent cluster of 4 incommensurate satellite reflections centreing each parent structure reciprocal lattice cell. The two sets of twin variant reflections comprising the overall composite EDP are labelled with superscripts 1 and 2 respectively. (b) A close to $\langle 14\bar{5}\rangle_R$ but essentially $\langle 111\rangle^*_R$ systematic row EDP of Sample B. The strong intensity of $\mathbf{G}\pm m\mathbf{q}$ satellite reflections running along the $\langle 111\rangle^*_R$ directions of reciprocal space is consistent with displacive shifts of the $(111)_R \equiv (003)_h$ metal atom layers along the $[111]_R \equiv [003]_h$ directions of real space.

incommensurate modulation can then only be associated with Sn/Sb ordering and/or displacements running along the $[111]_R \equiv [003]_h$ directions of real space.

The strong intensity of $\mathbf{G} \pm m\mathbf{q}$ satellite reflections running along the $\langle 111 \rangle_R^*$ directions of reciprocal space in essentially $\langle 111 \rangle_R^*$ systematic row EDPs such as that shown in Fig. 5b is quite consistent with displacive shifts of the $(111)_R \equiv (003)_h$ metal atom layers along the $[111]_R \equiv [003]_h$ directions of real space, as required by the above superspace group symmetry and as occurs in the case of elemental Sb itself. Note that these displacements could, in principle, be either directly correlated with, or independent of, associated Sn/Sb ordering. We presume the former is the case. Note also that fully occupied, non-mixed metal atom sites along the $[111]_R \equiv [003]_h$ stacking direction would necessitate a crenel, or square wave, type occupational Atomic Modulation Function (AMF) [25,26]. The observation of up to third-order harmonic satellite reflections in some EDPs (see e.g. Fig. 5b) suggests that the associated AMFs may indeed be non-sinusoidal. On the other hand, only first-order harmonic satellite reflections were observable in the synchrotron XRD data.

In addition to the incommensurate satellite reflections apparent in Figs. 4 and 5, there also exists a characteristic, highly structured diffuse intensity distribution in the form of sheets of diffuse intensity perpendicular to each of the three $\langle 001 \rangle_R^*$ directions of reciprocal space as is apparent from the (a) $\langle 001 \rangle_R$ and (b) $\langle \bar{1}14 \rangle_R$ zone axis EDPs shown in Fig. 6. Note that the diffuse streaking in Fig. 6a runs along the $[100]_R^*$ and $[010]_R^*$ directions of reciprocal space, that in Fig. 6b runs along the $[401]_R^*$ and $[04\bar{1}]_R^*$ directions of reciprocal space while that in Fig. 5b runs along the $[501]_R^*$ and $[054]_R^*$ directions of reciprocal space. In each case, the observed diffuse streaking is perpendicular to a $\langle 100 \rangle_R$ real space direction and, taken together, imply the existence of sheets of diffuse intensity perpendicular to each of the three $\langle 001 \rangle_R^*$ directions of reciprocal space.

Note also that the observed diffuse streaking is transverse polarized in that the intensity of the observed diffuse streaking is always strongest when looking out along directions of reciprocal space perpendicular to the direction of the streaking itself and goes to zero when looking along the direction of the streaking itself. This is obscured by multiple scattering in the case of the $\langle 001 \rangle_R$ zone axis EDP of Fig. 6a but is clearly apparent in the $\langle \bar{1}14 \rangle_R$ zone axis EDP shown in Fig. 6b. It implies the existence of $\langle 001 \rangle_R$ columns of atoms undergoing correlated displacement along $\langle 001 \rangle_R$ but with no transverse correlation from one such column to the next. The observed diffraction evidence requires that this must be happening along all three $\langle 001 \rangle_R$ directions simultaneously.

Finally, note that this additional structured diffuse distribution appears to be largely independent of the incommensurate modulation in that it does not run through the incommensurate satellite reflections (see e.g. Fig. 6b) but only through the Bragg reflections of the underlying average structure. This suggests that it does not arise from Sn/Sb ordering but is rather a fundamental property of the primitive, essentially simple cubic average structure.

4. Interpretation

4.1. The structured diffuse intensity

The transverse polarized structured diffuse intensity implies the existence of $\langle 001 \rangle_R$ columns of atoms undergoing correlated displacement along $\langle 001 \rangle_R$ but without transverse correlation from one such column to the next.

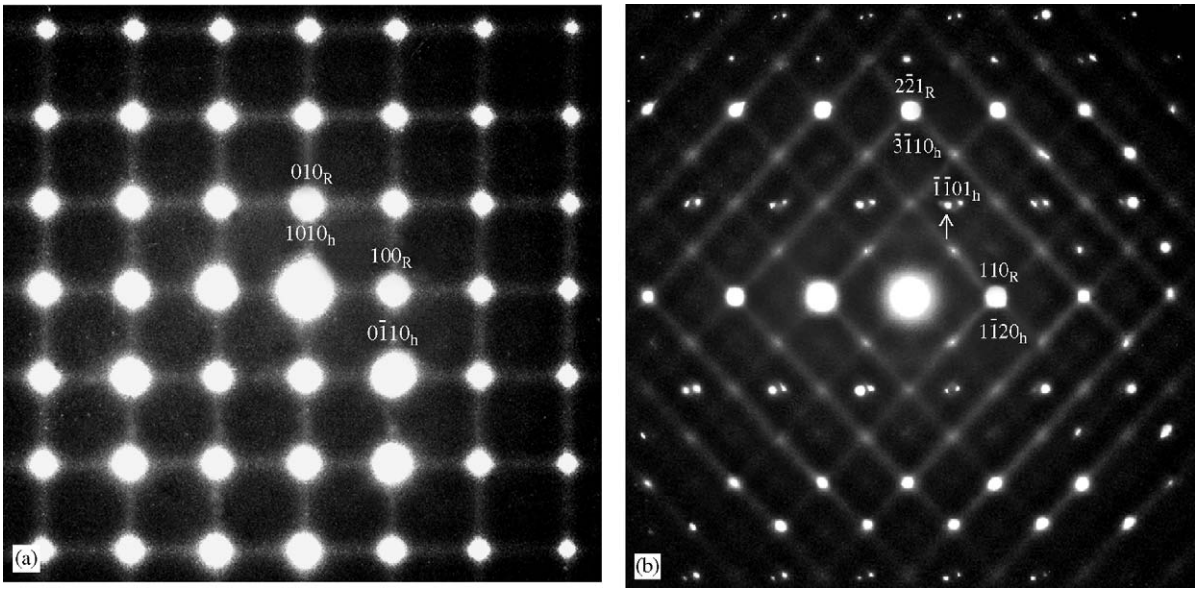

Fig. 6. (a) $\langle 001 \rangle_R$ and (b) $\langle \bar{1}14 \rangle_R$ zone axis EDPs typical of the "SnSb" phase. Note the characteristic, highly structured diffuse streaking perpendicular to each of the three $\langle 001 \rangle_R$ directions of real space.

We believe the origin of this behaviour can be found in the Rigid Unit Mode (RUM) theory of Dove and his collaborators [27] who have shown that inherent instability results if the degrees of freedom in a system are greater than the local constraints operating upon that system. One of the very simple examples they give of such a system is that of four rods hinged at the corners (see Fig. 2 of [27]), essentially a two-dimensional version of a primitive simple cubic structure. They show that such a structure is unstable against transverse shear modes [27]. In the present context, if we ignore the incommensurate modulation associated with the Sn/Sb ordering and the associated (very slight) rhombohedral metric distortion of the originally primitive cubic structure, an instability to transverse shear waves implies $\langle 001 \rangle_R$ columns of metal atoms undergoing rigid body rod-like displacements along $\langle 001 \rangle_R$ but without transverse correlation from one such column to the next—just as is observed experimentally (see e.g. Fig. 6).

The implication is that any simple cubic (or close to simple cubic) structure would be unstable against such transverse shear waves. The only known elemental metal with a simple cubic structure at room temperature is α-Po (not exactly a readily available metal) which may explain why the structured diffuse scattering found in this paper does not appear to have been reported before in any metallic system, as least as far as the authors are aware.

4.2. The incommensurate structure

Given the simplicity of the underlying average structure (only one metal atom site per primitive parent unit cell), the $R\bar{3}m$ (0, 0, ~1.311) superspace group symmetry and the fact that only first-order harmonic satellite reflections are observed in our experimental XRD data, it is clear that the $\mathbf{q}_h = 1.3109(9)\mathbf{c}_h^*$ modulation can only be associated with sinusoidal-type Sn/Sb ordering and/or displacive shifts of successive $(001)_h$ metal atom layers along the $\mathbf{c}_h = \frac{1}{3}[111]_R$ direction of the $R\bar{3}m$ average structure. Note that the internal co-ordinate $\bar{x}_4 = \mathbf{q}_h.(\mathbf{r}_h + \mathbf{t}_h) = \frac{1}{3}nq_h = 0.437n$ in the current case, where the integer n labels successive metal atom planes perpendicular to $\mathbf{c}_h$ [24–26].

The assumed cosinusoidal occupational atomic modulation function (AMF) as a function of $\bar{x}_4 = 0.437n$ modulo an integer is shown in Fig. 7a while the refined sinusoidal displacive AMF as a function of $\bar{x}_4$ is shown in Fig. 7b. For ease of understanding in 3-d space, the $\bar{x}_4$ position of successive metal atom layers are labelled as $n = 0, 1, 2$, etc. in Fig. 7. Fig. 7c then shows the magnitudes of the displacements of the successive metal atom layers as a function of n. The filled and empty circles in Fig. 7c represent Sb- and Sn-rich metal atom layers respectively while the grey circles represent close to 50:50 occupied layers. Note that the predicted arrangement of $(0\,0\,1)_h$ layers is largely an alternating sequence of Sn- and Sb-rich layers. Occasionally, however, a double layer of either Sn-rich or Sb-rich layers must occur. When a Sn-rich double layer occurs, it is clear from Fig. 7 that the relative distance between those layers increases relative to the average while the reverse will clearly be the case for Sb-rich double layers. It is significant that the distance of closest approach of Sb atoms in elemental Sb is ~2.91 Å [28] as compared to the ~3.066 Å metal atom separation distance in the current unmodulated parent structure. This might provide an explanation as to why neighbouring Sb-rich layers might dimerize as appears to be the case.

While the above proposed explanation for the modulated structure of 'SnSb' is conceptually very appealing, the problem with it is that it implies a strict correlation between chemical composition and $\mathbf{q}_h$. A composition of $Sn_{0.5-x}Sb_{0.5+x}$ should be associated with a $\mathbf{q}$ of $3(0.5-x)$.

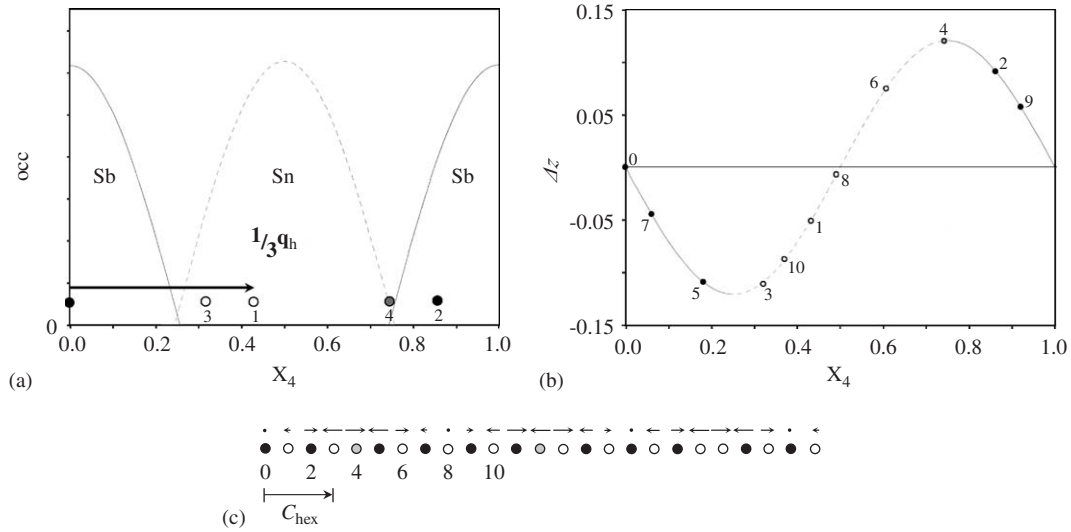

Fig. 7. The cosinusoidal occupational AMF as a function of $\bar{x}_4$ is shown in (a) while the refined sinusoidal displacive AMF is shown in (b). For ease of understanding in 3-d space, the $\bar{x}_4$ position of successive metal atom layers are labelled as $n = 0, 1, 2$, etc. (c) shows the magnitudes of the displacements of successive metal atom layers. The filled and empty circles represent Sb- and Sn-rich metal atom layers, respectively while the grey circles represent close to 50:50 occupied layers.

Experimentally, however, this does not appear to be the case (cf. e.g. Fig. 2 with the experimental reproducibility of the primary modulation wave-vector $\mathbf{q}_h$). Given that both Sn and Sb, as pure elements, themselves can dissolve ~10 atomic per cent of the other species [16], it may be that allowing the individual $(001)_h$ layers to vary from strict Sn or Sb stoichiometry provides a mechanism whereby $\mathbf{q}$ need not be directly related to composition. Nonetheless an explanation needs to be found for the remarkable experimental reproducibility, and sharpness, of the observed incommensurate primary modulation wave-vector magnitude.

Acknowledgments

R.L.Withers and S.Schmid thank the Australian Research Council (ARC) for the financial support in the form of an ARC Discovery Grant. R.L. Withers and F.J. Brink thank the ANU Electron Microscope Unit for access to equipment. Help and financial support for the collection of the synchrotron data was obtained through the Australian Synchrotron Research Program (ANBF Proposal 04/05-AB-03) and is gratefully acknowledged.

References

[1] G.P. Secundus, Naturalis Historia, Book XXXIII, xxxiv (#101) (~77 CE).
[2] http://www.vanderkrogt.net/elements/elem/sb.html.
[3] G. Agricola, De Re Metallica, Basel, 1556.
[4] J. Thölde (Basilius Valentinus), Triumph-Wagen Antimonii, J. Apel, Leipzig, 1604.
[5] G.P. Secundus, Naturalis Historia, Book XXXIII, xxx (#94) (~77 CE).
[6] C.-S. Oh, J.-H. Shim, B.-J. Lee, D.N. Lee, J. Alloys Compd. 238 (1996) 155–166.
[7] P.J.T.L. Oberndorff, A.A. Kodentsov, V. Vuorinen, J.K. Kivilahti, F.J.J. van Loo, Ber. Bunsen-Ges. Phys. Chem. 102 (1998) 1321–1325.
[8] M. Abtew, G. Selvaduray, Mater. Sci. Eng. 27 (2000) 95–141.
[9] Abu Bakr El-Bediwi, Cryst. Res. Technol. 40 (7) (2005) 688–691.
[10] J. Yang, M. Wachtler, M. Winter, J.O. Besebhard, Electrochem. Solid-State Lett. 2 (4) (1999) 161–163.
[11] I. Rom, M. Wachtler, I. Papst, M. Schmied, J.O. Besenhard, F. Hofer, M. Winter, Solid State Ionics 143 (2001) 329–336.
[12] A. Osawa, Nature 124 (1927) 14.
[13] V. M. Goldschmidt, Geochemische Verteilungsgesetze, vol. viii, 1927.
[14] W. Morris Jones, E.G. Bowen, Nature 126 (1930) 846–847.
[15] E.G. Bowen, W. Morris Jones, Philos. Mag. 12 (1931) 441–462.
[16] G. Hägg, A.G. Hybinette, Philos. Mag. Ser. 7 20 (1935) 913–929.
[17] C.A. MacKay, J. Appl. Crystallogr. 2 (1969) 295–297.
[18] V. Vassiliev, M. Lalaurain, J. Hertz, J. Alloys Compd. 247 (1997) 223–233.
[19] E.P. Nikolaeva, V.A. Grigorenko, S.D. Gagarkina, P.Y. Tsypkina, Zap. Vseross. Mineral. Ova. 99 (1970) 68–70.
[20] D. Rose, Neues Jahrb. Mineral. Monatsh. 3 (1981) 117–126.
[21] B. Noläng, Inst. Materialkemi, Ångströmlaboratoriet, Uppsala Universitet, Box 538, S-751 21 Uppsala, Sweden.
[22] V. Petříček, M. Dušek, The Crystallographic Computing System JANA2000, Institute of Physics, Praha, Czech Republic, 2000.
[23] M. Dušek, V. Petříček, M. Wunschel, R.E. Dinnebier, S. van Smaalen, J. Appl. Crystallogr. 34 (2001) 398–404.
[24] T. Janssen, A. Janner, A. Looijenga-Vos, P.M. de Wolff, Incommensurate and commensurate modulated structures, in: A.J.C. Wilson (Ed.), International Tables for Crystallography, vol. C, Kluwer Academic Publishers, Dordrecht, 1995, pp. 797–835.
[25] S. van Smaalen, Crystallogr. Rev. 4 (1995) 79–202.
[26] R.L. Withers, S. Schmid, J.G. Thompson, Prog. Solid State Chem. 26 (1998) 1–96.
[27] A.P. Giddy, M.T. Dove, G.S. Pawley, V. Heine, Acta Crystallogr. A 49 (1993) 697–703.
[28] B.D. Cullity, Elements of X-ray Diffraction, Appendix 5, second ed, Addison-Wesley, Reading, MA, 1978.